Al-Farouk journal of sciences
Volume (2), Issue (3) (JUNE, 2026)
ISSN: 3135-2359

مجلة الفاروق للعلوم
المجلد (2) العدد 3 يونيو 2026
ردمد: 3135-2359

Fabricated of Doping and Co-doing Cadmium Sulfide (CdS) Thin Films via Spray Pyrolysis for High-Efficiency Photovoltaic Window Layers (2015–2025) :A Comprehensive Review Artical

Foziah Abdullah Almawal[1], Yousef Al-Naas[2]
[1]Department of chemistry, Factually of Education, University of Zawia, Al Ajelat, Libya.
F.Almawal@Zu.edu.ly
ORCID:0009-0007-1292-228X
[2]The Libyan Center of Solar Energy Researchers and Studies, Tripoli, Libya.
yousef.waheshi@gmail.com

تاريخ الاستلام: 2026/04/07 تاريخ المراجعة 09/05/ 2026 تاريخ القبول:2026/05/20- تاريخ النشر: 09/06/ 2026

Abstract:
This review provides a comprehensive quantitative and systematic analysis of the development of spray-deposited, doped, and co-doped cadmium sulfide thin films used as optical windows in solar cells during the period from 2015 to 2025. Based on 25 peer-reviewed studies, this work classifies a wide range of dopers into: Group III elements (aluminum, gallium, indium), Group I acceptors (sodium, silver, copper), transition metals (barium, nickel, cobalt, manganese, zinc), rare earth elements (europium, praseodymium, dysprosium), and synergistic co-doping systems (aluminum-sodium, gallium-potassium, magnesium-cobalt, tin-zinc, aluminum-lanthanum). Analysis of variation reveals that the resulting stable hexagonal phase (wurtzite) is present in 72.0% of published studies. Quantitative scanning spectroscopy identifies an optimal doping window at μ=3.00 atomic. With an ±0.81% (σ=±0.81% atomic), this achieves a blueshift in the optical band gap (according to Burstein-Moss) averaging 2.45 eV (σ=±0.02 eV) and a transparency of 70–85%. Exceeding this value leads to the deposition of amorphous secondary phases at the grain boundaries, generating lattice stress and a 56.0% reduction in grain size (<30 nm). Donor doping (aluminum, fluorine) yielded the best results in conductivity and device efficiency, while rare-earth elements (dysprosium, praseodymium, europium) improved the performance of the photodetectors. However, the data revealed a critical gap in transport data (0.0% for Hall kinetics measurement) and widespread neglect (88.0%) of long-term environmental degradation protocols.

Keywords: Cadmium Sulfide – Doping - Co-doping - Spray Pyrolysis -Thin Films – Photovoltaics - Window Layer.

Introduction:

Solar cells convert sunlight directly into electricity using the photovoltaic effect, providing a low-cost, near-permanent energy source without the need for intermediate energy conversions **(1).** The global shift towards sustainable energy has increased the focus on thin-film photovoltaics, where cadmium sulfide (CdS) is used as the primary window layer due to its unique properties, such as a 2.42 eV energy band gap, strong absorption, and chemical stability **(2).**

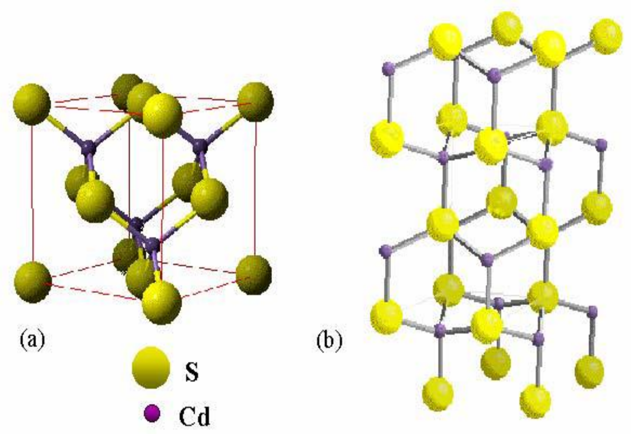

Fig. 1 The crystal structure of CdS (a) cubic zinc-blend (b) hexagonal wurtzite (3).

Doping modifies the properties of semiconductors by adding foreign atoms to alter their electronic and optical characteristics **(4).** Co-doping is an advanced strategy that simultaneously improves multiple material properties by enhancing the solubility of the doped material and the stability of defects, a field that has been extensively studied over the past two decades **(5)**. Thermal spray pyrolysis decomposition is an ideal method for depositing CdS thin films due to its cost-effectiveness, scalability, and precise parameter control. This allows for precise control of the membrane properties, such as shape, crystallinity, and transparency, which directly improves the performance of the photovoltaic cell **(6).**

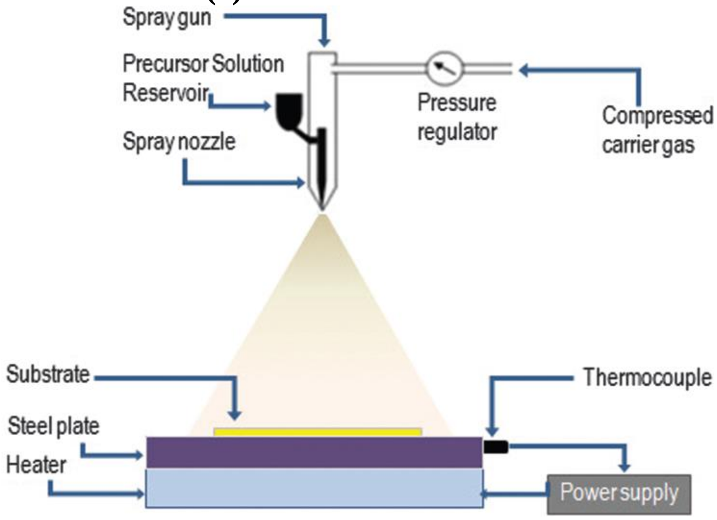

Fig.2. Schematic diagram of spray pyrolysis system for the preparation of CdS nanocomposites thin films (7).

The main objective of this work is to comprehensively analyze the development of doped and co-doped cadmium sulfide thin films over the past decade (2015–2025), evaluate their performance in photovoltaic devices, identify current challenges, and suggest future research directions with a particular focus on applications in areas with high solar irradiance such as Libya.

Methodology and Scope:

This study systematically reviews peer-reviewed articles and reference research published between 2015 and 2025. All the papers were acquired from international scientific databases, including Scopus and Web of Science. The scope of the study includes research on single-element doping (e.g., Aluminum, Gallium, Indium, Copper, Silver, Manganese, Fluorine, Europium, Praseodymium, Dysprosium, etc) and co-doping systems (e.g., Aluminum-Sodium, Gallium-Potassium, Manganese-Copper, Magnesium-Cobalt, etc), focusing on changes in structural, morphological, optical, and electrical properties. The systematic review was limited to studies that used spray pyrolysis as the deposition technique. This study comprises a discussion of single-element doping strategies, followed by co-doping approaches, a comparative performance analysis, an identification of research gaps, and finally, an examination of challenges and future prospects.

1. Yılmaz et al, (2015) conducted a study entitled "Comparative studies of CdS, CdS:Al, CdS:Na and CdS:(Al–Na) thin films prepared by spray pyrolysis" . They deposited undoped, Al-doped, Na-doped, and Al–Na co-doped CdS thin films using spray pyrolysis. XRD results showed all films had a hexagonal wurtzite structure, while SEM revealed Al doping promoted grain growth, and Na or co-doping caused porous small-grain morphology. Optical studies indicated that Al doping increased the band gap to 2.42 eV, whereas Na and co-doping reduced it, photoluminescence increased with Al but decreased with Na and co-doping, Electrical measurements showed Al-doped films had the highest carrier concentration and lowest resistivity, while co-doping slightly reduced carrier concentration and increased resistivity **(8).**
2. In 2016, Jinzhan Su, conducted a study titled "Synthesis of Cu-doped CdS microspheres via ultrasonic spray pyrolysis and their enhanced photocatalytic activity". Here, Cu-doped CdS microspheres were synthesized using ultrasonic spray pyrolysis and tested for their morphological photocatalytic performance with scanning electron microscopy (SEM), X-ray fluorescence-spectrometry (XRF), UV-Vis absorption spectra and X-ray diffraction (XRD) . They found that smaller CdS particles had better photocatalytic hydrogen production. With Cu doping at ~0.5 mol %, the bandgap increased and surface defects decreased, leading to enhanced hydrogen evolution under alkaline conditions (pH 13.2) using sacrificial donors **(9).**
3. In 2016, Yılmaz et al, carried out a study entitled "Physical properties of CdS:Ga thin films synthesized by spray pyrolysis technique." In this research, CdS thin films were doped with Ga using the spray pyrolysis method, varying the Ga concentration from 0 to 8 at %. The results revealed that Films maintained a hexagonal (101) structure. 2-4 at%. Ga yielded the best results, improved transparency, slight bandgap increase (to ~2.43 eV), highest carrier density, and lowest resistivity. Higher Ga levels (6–8 at.%) causes a poor (~2.39 eV) optical transmission and electrical performance **(10).**
4. In 2016**,** Yılmaz et al, published another study entitled "Enhancement in the optical and electrical properties of CdS thin films through Ga and K co-doping." Here, CdS films were co-doped with Ga and K are grown on glass substrates at a temperature of 400 °C through spray pyrolysis. The findings all films exhibited a hexagonal crystal structure, though K doping degraded crystal quality, just as Ga concentration is fixed 2 at% for all CdS thin films, the best optical transparency in the visible region occurred at 4 at %. K, with a widened bandgap (~2.45 eV) compared to CdS:Ga (~2.43 eV). it can be deduced that 4 at% K-doped CdS:Ga thin films show the best optical and electrical behavior, which can be utilized for solar cell devices **(11).**
5. In 2017, Mohamed Bakr Mohamed et al, carried out a study titled "Effect of preparation methods and doping on the structural and tunable emissions of CdS." This research explored how preparation atmosphere and doping elements, specifically: Fe, Mn, and Mg affect cadmium sulfide (CdS) thin films. They used thermolysis under air and nitrogen atmospheres and found all CdS samples displayed both cubic and hexagonal phases, with larger crystallite sizes when prepared under nitrogen.

Optical analysis showed that films made in air exhibited a blue-shifted photoluminescence (PL), while all doped samples showed red shifts compared to undoped ones. Emissions varied by dopant: Fe- and Mg-doped films emitted violet and blue light; Mn-doped films in air showed violet, blue, and yellow emissions, whereas under nitrogen they displayed violet, blue, and green emissions **(12).**

6. In 2017 R. Murugesan et al, conducted a study titled "Structural, Optical and Magnetic Properties of Ba- and Ni-Doped CdS Thin Films Prepared by Spray Pyrolysis Method" They investigated the structural, optical, and magnetic properties of barium (Ba) and nickel (Ni)-doped cadmium sulfide (CdS) thin films prepared by spray pyrolysis. The films were deposited on glass substrates at 400 °C and analyzed using X-ray diffraction (XRD), scanning electron microscopy (SEM), optical spectroscopy, and vibrating sample magnetometry (VSM). XRD results revealed that all films exhibited a cubic crystal structure with a preferred orientation along the (111) plane. The crystallite size increased from 31 nm in pure CdS to 33 nm in Ba-doped and 45 nm in Ni-doped films. Optical measurements indicated a decrease in the energy bandgap from 2.43 eV in pure CdS to 2.1 eV with Ba doping. Photoluminescence spectra showed a strong emission peak at 517 nm for pure CdS, with a slight red shift observed upon doping. VSM studies revealed that both Ba and Ni doping induced magnetic behavior in the CdS films **(13).**
7. In 2018, Yılmaz et al, conducted a study titled "Optical and Electrical Optimization of Dysprosium-Doped CdS Thin Films," In this research investigate the impact of dysprosium (Dy) doping on the structural, optical, and electrical properties of cadmium sulfide (CdS) thin films prepared via spray pyrolysis method on glass substrates. Doping concentrations ranged from 1 to 5 at %. X-ray diffraction (XRD) analysis revealed that all films exhibited a hexagonal crystal structure. The preferred orientation was along the (101) plane for undoped and 1–2 at % Dy-doped films, Higher Dy concentrations (3–5 at%) led to a more random orientation, with the (002) plane becoming dominant at 5 at % Dy. The crystallite size progressively decreased from 39 to 27 nm with increasing Dy doping. Optical measurements showed that the 5 at % Dy-doped films possessed the highest transmittance (over 80%) among all samples. Except for the 2 at % Dy-doped sample, the other films exhibited a bandgap of approximately 2.45 eV. Photoluminescence results indicated that more stoichiometric films were formed after Dy incorporation **(14).**
8. In a 2018 study, Shadia Ikhmayies et al, conducted a study titled "A study of the absorption edge of CdS:In thin films prepared by spray pyrolysis". They investigated the absorption edge of indium-doped cadmium sulfide (CdS:In) thin films prepared by spray pyrolysis on glass substrates at 490°C. X-ray diffraction (XRD) and scanning electron microscopy (SEM) analyses revealed that the films exhibited a polycrystalline structure, predominantly in the wurtzite hexagonal phase, with some indications of the cubic zinc blende phase. Optical transmittance measurements were conducted in the wavelength range of 400–1100 nm, and the second derivative of the absorbance spectrum was analyzed to identify the free exciton peaks associated with the wurtzite phase. The A and B free exciton peaks merged into a single peak, while the C free exciton peak remained distinct. These findings were compared with existing literature, and the observed peak separations were found to be in good agreement with previously reported values **(15).**
9. In a 2018 study, El Radaf, et al, investigated research titled "Synthesis and Characterization of F-doped CdS Thin Films by Spray Pyrolysis for Photovoltaic Applications", They employed a spray pyrolysis method to deposit both pure and fluorine-doped (F:CdS) cadmium sulfide thin films on pre-heated glass substrates. X-ray

diffraction confirmed that both sets of films maintained a cubic crystal structure, regardless of the fluorine content. The researchers evaluated both the linear optical properties—such as refractive index and bandgap—and nonlinear ones (third-order susceptibility $\chi^{(3)}$ and nonlinear refractive index n_2). Their results showed that a 8 wt% fluorine doping yielded the highest absorption coefficient and optical conductivity among all tested concentrations. Building on this, they incorporated the 8 wt% F:CdS film into an Al/p-Si/F:CdS/Au heterojunction, achieving a notable improvement in photovoltaic performance—from 1.92% to 2.63%. This highlights the significant impact of fluorine doping in enhancing both optical and photovoltaic properties of CdS films for optoelectronic device applications **(16).**

10. In 2018, Karrar. Mahdi. Saleh conducted study titled" Influence of Substrate Temperature on Structural Properties of CdS Thin Films Prepared by Chemical Spray pyrolysis". The current work, CdS thin films are designed by the chemical spray paralysis method on glass substrates, which is designed to study the impact of substrate temperature on the structure properties of prepared films, with a constant thickness (440 ± 10 nm) with a separate temperature from cadmium nitrate. The results of structural measurements shown through (SEM) for the symmetry of prepared films, and the results of (AFM) are the same to compose nanopathy and the average rough value of the average roughness (RMS) (RMS) (0.699nm). And X-ray diffraction patterns have shown that all movies are the size of grain within the boundary of polycrystalline, hexagonal structure, nano scale, and the substrate does not affect the crystal structure of the temperature films **(17).**
11. In 2019, S. Yılmaz et al, conducted a study titled "A research on growth and characterization of CdS:Eu thin films". Eu-doped CdS via spray pyrolysis including various quantities of Eu atoms (from 0 to 10 at%), were synthesized on glass slides. The researchers focused on optimizing Eu doping levels to enhance film quality. The crystallite size decreased from 36.2 nm to 32.4 nm with increased Eu doping. Optical measurements revealed a maximum transmittance of 68% at 820 nm and a bandgap reduction from 2.58 eV to 2.47 eV. Electrical properties improved with Eu doping up to 6 at %, enhancing carrier density and reducing resistivity, but declined with higher doping levels. These findings suggest that Eu doping optimizes both optical and electrical properties of CdS thin films for optoelectronic applications **(18).**
12. In 2019, R. Murugesan et al, investigated study titled "Effect of Mg/Co on the properties of CdS thin films deposited by spray pyrolysis technique". They prepared Mg, Co doped and (Mg, Co) co-doped CdS thin films were using chemical spray pyrolysis method and observed from the X-ray diffraction study that the film (111) displays the cubic stage of the CdS with a favorite orientation with the aircraft and confirmed the analysis and XPS analysis that spread energy to the inclusion of Mg and Co. Doped and co-doped CdS confirmed by Raman spectrum display 1l0 and 2l0 vibrations. The core level XPS spectra ensures the inclusion of doping elements properly. CdS has been seen by FE-SEM due to the inclusion of Co and MG in thin films. Particle size and crystalline nature is manifested with HRTEM images and the same SAED pattern. Cum-decorated CdS show a significant shift blue in thin films absorption spectrum. Cum-dopped CdS have seen better magnetic properties for thin films. **(19).**
13. In 2019, Ahmed Aboud et al, carried out a study titled "The effect of Cu-doping on CdS thin films deposited by spray pyrolysis." They focused on Cu-doped CdS thin films. The researchers studied spray pyrolysis-produced CdS thin films along with Cu-doped CdS thin films with 2%, 4%, and 6% Cu. The researchers used

XRD, XPS, AFM, UV–Vis spectroscopy, and DC-conductivity to discover that Cu doping produced a minor decrease in particle size (from ~28 nm to ~25.4 nm). The XRD data enabled researchers to calculate how Cu doping modified the internal stress and dislocation density of the samples. The surface roughness of samples increased from 25 nm to 31 nm when doping reached 6% according to SEM and AFM analysis. The bandgap showed a slight reduction from 2.43 eV to 2.39 eV while all films presented semiconducting characteristics during electrical testing and Cu-doping increased activation energy. **(20).**

14. Shkir et al, (2020), conducted a study titled " A remarkable effect of Pr doping on key optoelectrical properties of CdS thin films prepared using spray pyrolysis technique for high-performance photodetector applications." They investigated how praseodymium (Pr) doping through chemical spray pyrolysis affects the optoelectrical properties of CdS thin films made by spray pyrolysis. They obtained densely packed nanostructured films that exhibited 19 to 32 nanometer crystallite sizes with a hexagonal crystal structure and 70 to 80 percent transparency. The addition of 5 wt% Pr to CdS films resulted in substantial improvements in dark current and photocurrent responses, which resulted in a responsivity value of 2.71 A/W and specific detectivity of 6.9×10^{11} Jones, 43 times better EQE, and an on/off switching ratio of 395, making them excellent candidates for photodetection applications. **(21).**
15. In a 2020 study, Manthrammel et al. investigated aluminum (Al)-doped Cadmium Sulfide (CdS) thin films fabricated via a cost-effective spray pyrolysis method. Their research confirmed the homogeneous distribution of Al within the films, which possessed a hexagonal crystal structure with crystallite sizes ranging from 16 to 22 nm. The study highlighted that Al-doping modified the surface morphology and significantly enhanced the material's third-order nonlinear optical properties, including its nonlinear susceptibility and refractive index, demonstrating its strong potential for future optoelectronic applications **(22).**
16. In 2021 Zina M. Shaban et al, conducted an earlier study titled “Structural, Morphology and Optical properties of Ag-doped Nanostructured CdS thin films.” They explored how silver (Ag) doping modifies the structural and optical properties of CdS thin films which were synthesized through chemical spray pyrolysis. The researchers added 1 wt% and 3 wt% of Ag to the films before performing XRD, AFM and UV-VIS characterization. The (020) plane represented the main XRD peak while the CdS films with 3% Ag doping showed the largest grain size. Ag doping decreased both strain values (from 25.23 to 21.10) and dislocation density values (from 53.04 to 37.08). The AFM images demonstrated that increasing Ag content reduced the grain size from 58.1 to 45.8 nm and surface roughness (RMS) decreased from 9.81 to 5.42 nm. Optical measurements showed that higher Ag content in the samples led to decreased transmittance and bandgap values (from 2.47 eV to 2.37 eV) while the absorption coefficient increased. The study demonstrates that Ag doping serves as an efficient method to modify CdS film characteristics for optoelectronic applications **(23).**
17. In a 2021 study Zein K. Heiba et al, titled "Effect of Mn-doping on the optical and electronics characteristics of cadmium sulfide photocatalyst prepared under different conditions". Using a thermolysis method, both pure and Mn-doped CdS were synthesized in air and under nitrogen. Analysis showed that Mn-doping did not alter the dual-phase (hexagonal and cubic) crystal structure but did affect lattice parameters. Optically, Mn-doping caused a consistent redshift in the band gap, enhancing light absorption at longer wavelengths. Density functional theory

(DFT) calculations revealed unique electronic behaviors. Mn-doped CdS with a cadmium deficiency exhibited half-metallic properties, while samples with a sulfur deficiency showed enhanced optical conductivity in the visible range **(24).**

18. In a 2022 study Gbashi and Alzubaidi fabricated and investigated nanostructured films for optoelectronic applications, titled "Zn–doped and (Sn: Zn) co-doped CdS nanostructures for optoelectronics,". They first synthesized Zn-doped and Sn:Zn co-doped CdS nanostructures via a chemical reaction and then deposited them as thin films using a pulsed laser method. Their results showed that the films had a hexagonal phase with very fine nanocrystallites (2.6–2.85 nm). The study found that doping with Zn increased the optical energy gap to 3.30 eV. Furthermore, electrical examinations revealed that co-doping with Sn enhanced the current, which was attributed to the creation of new electronic sub-levels. Morphological analysis indicated that the films were quite smooth, with surface roughness increasing with the addition of co-doping ions. **(25).**
19. Trabelsi et al. (2022) conducted a study titled "A comprehensive study on Co-doped CdS nanostructured films fit for optoelectronic applications." The research explored the preparation of cobalt-doped CdS nanostructures using spray and nebulizer-based deposition techniques, focusing on their suitability for device integration. The results demonstrated that Co doping effectively tailored the optical bandgap and electrical conductivity. The optimized films exhibited device-relevant optoelectronic performance, making them promising for next-generation applications **(26).**
20. Khan et al. (2023) carried out a study titled "Enhanced nonlinear and photodetection response of Zn-doped CdS thin films prepared by spray pyrolysis." This work examined the dual role of Zn doping in enhancing photodetector response and nonlinear optical behavior. The findings showed that defect passivation through Zn incorporation improved photoluminescence (PL) and responsivity. An optimal Zn concentration was found to balance carrier density and optical transparency, enabling effective device performance without sacrificing light transmission **(27).**
21. Gezgin et al. (2023) conducted a study titled "Numerical analysis of thin-film solar cells based on In-doped CdS semiconductor." The research used device simulations to evaluate In:CdS window layers in thin-film solar cells. The findings predicted efficiency improvements through optimization of indium doping levels and film thickness, providing valuable guidelines for future experimental designs **(28).**
22. Kamatam et al. (2024) connected a study titled "Fabrication of Al and La co-doped CdS thin film for ammonia gas-sensing via low-cost nebulizer spray." The work explored co-doping of aluminum (Al) and lanthanum (La) in CdS thin films for ammonia gas sensor applications. The results showed a synergistic improvement in sensor sensitivity and response time, accompanied by microstructural densification that contributed to performance gains **(29).**
23. Mohammed (2025) conducted a study titled "Characteristics of CdS thin-film nanoparticles fabricated via spray pyrolysis deposition." The research focused on the controlled growth of nanoscale CdS particles using spray pyrolysis. Findings showed improved optical quality and identified process parameters to ensure reproducible nanoparticle synthesis **(30).**
24. Molina-Jiménez et al. (2025) carried out a study titled "Ultra-thin films of CdS doped with silver: Synthesis and modification of optical, structural, and morphological properties by doping concentration effect." The study examined the effects of varying silver doping levels on ultra-thin CdS films **(31).**

25. John et al. (2025) conducted a study titled "Optical, structural and morphological characterization of indium-doped CdS (CdS:In) thin films for photovoltaic cell applications." The work benchmarked CdS:In films for photovoltaic suitability. The study found higher optical transmittance and reduced defect-related tailing, confirming their applicability in PV cells **(32).**

Table 1: Physical Benchmarks of Undoped Spray-Pyrolyzed CdS Thin Films:

Material	Reference(s)	Structural Properties (Phase, Crystallite Size *D*)	Optical Properties (Bandgap *Eg*, PL)	Electrical Properties (Resistivity *ρ*, Carrier Conc. *n*)
Pure CdS (Baseline)	Yılmaz et al. (2015); Murugesan et al. (2017); Saleh (2018)	Polycrystalline structure; primarily hexagonal wurtzite or Cubic phase; *D*=31–40 nm.	*Eg*=2.42–2.47 eV; exhibits a sharp, distinctive photoluminescence (PL) peak near 517 nm.	$\rho \sim 10^4$–10^5 Ω·cm; $n \sim 10^{12}$–10^{16} cm^{-3} (High inherent resistivity).

- This table represents the "control group" or experimental baseline. The success or failure of any doping process can only be determined by referring to the values listed in this table.
- Crystal structure: Pure films typically exhibit a polycrystalline structure, either in the wurtzite or cubic phase, with a grain size ranging from 31 to 40 nm, which is the typical size for thermal growth of CdS.
- Optical Properties: The film has a natural optical gap between 2.42 and 2.47 eV, which is ideal and gives the film a yellowish tint, with peak optical clarity at a wavelength of 517 nm. Electrical Deficiency (Major Problem): The table shows that these pure films have very high electrical resistivity (10^4–10^5 Ω·cm) and a severe deficiency of charge carriers (10^{12}–10^{16} cm^{-3}). This poor conductivity is the main reason why all the researchers in the following tables perform doping.

Table 2: Structural, Optical, and Electrical Variations via Single-Element Doping:

Dopant Category	Reference(s)	Structural Properties (Morphology, Crystallite Size *D*)	Optical Properties (Bandgap *Eg*, Transmittance *T*%)	Electrical & Device Properties (Resistivity *ρ*, Carrier Conc. *n*, Efficiency *η*)
Group III Donors (Al, Ga, In)	Yılmaz et al,(2015, 2016) Ikhmayies et al, (2018) Manthrammel et al, (2020) John et al, (2025)	Hexagonal structure maintained; Al enhances grain size; Ga is optimal at 2–4 at %; In displays mixed phases.	*Eg* expands to 2.42–2.48 eV; Highly transparent (*T*=70–85%); Exciton peaks identified for In.	**Al:** $\rho \sim 10^{-2}$ Ω·cm, $n \sim 10^{19}$ cm^{-3} **Ga:** $\rho \sim 10^{-1}$ Ω·cm, $n \sim 10^{18}$ cm^{-3} PV window layer compatibility confirmed.

Non-Metal Donor (Fluorine - F)	El Radaf et al. (2018)	Stable cubic zinc-blende crystal structure strictly maintained across all F levels.	*Eg*~2.40 eV; *T*=65–75%; Max absorption at 8 wt.%; Exhibits non-linear optics ($\chi(3)$, *n*2).	Direct PV device integration: Heterojunction solar cell efficiency boosted from **1.92%→2.63%** (+37%).
Group I Acceptors (Na, Ag, Cu)	Yılmaz et al, (2015) Su (2016) Aboud et al, (2019) Shaban et al, (2021) Molina-Jiménez et al. (2025)	Na induces porous structures. Ag reduces *D* (58→46 nm). Cu decreases *D* (28→25.4 nm).	Triggers bandgap narrowing (Redshift); Ag: 2.47→2.37 eV; Cu: 2.43→2.39 eV; *T*% degrades.	**Na**: ρ↑, *n*↓. **Cu:** Increases thermal activation energy (*Ea*). **Ag/Na:** Quantitative electrical metrics omitted.
Transition Metals (Ba, Ni, Co, Mn, Zn)	Murugesan et al, (2017) Heiba et al. (2021) Khan et al. (2023)	Cubic (111) orientations; *D*=33 nm (Ba), 45 nm (Ni) ; Zn induces grain defect passivation.	Ba severely narrows *Eg* →2.1 eV; Mn induces a redshift; Zn-only expands *Eg* →3.30 eV with high PL.	Diluted magnetic semiconductor (DMS) behavior induced (Ba, Ni). Zn enhances photodetector responsivity.
Rare Earth Luminescent Ions (Eu, Pr, Dy)	Yılmaz et al. (2018, 2019) Shkir et al. (2020)	Hexagonal wurtzite, Gradual reduction in size: Dy: 39→27 nm. Eu: 36→32 nm. Pr: 19–32 nm.	**Dy:** Highly transparent (T > 80 %), *Eg*~2.45 eV **Eu:** *Eg* reduce 2.58→2.47 eV **Pr:** *T*~70–80%, *Eg*~2.45 eV.	**Eu:** ρ↓ up to 6 at % . (n~1017 cm^{-3}). **Pr:** Superior photodetector metrics; Responsivity =2.71 A/W, 43× EQE boost.

- Table (2) shows the most successful combination for solving the electrical problem described in Table 1, using the "negative donor doping" mechanism.
- Physical explanation of the mechanism: When Group III elements (Al^{3+}, Ga^{3+}, In^{3+}) are introduced, they replace divalent cadmium ions (Cd^{2+}) within the crystal lattice. This substitution leaves an additional free electron from each doped atom, resulting in a significant increase in the free electron concentration to (10^{18} –10^{19} cm^{-3}). Consequently, the electrical resistivity decreases significantly from 10^5 (in Table 1) to (10^{-1}–10^{-2} Ω·cm).
- Dual optical effect: In addition to the electrical enhancement, these impurities widen the optical band gap (2.42–2.48 eV) due to a well-known physical phenomenon called the Burstein-Moss effect. In this effect, energy levels near the bottom of the conduction band are filled with electrons, forcing electrons from the valence band to jump a greater distance (higher energy). This is ideal for the optical layer in solar cells, allowing more sunlight to pass through without parasitic absorption.

Table 3: Comparison of Group I Acceptors (*p*-type / Compensation Behavior):

Property / Metric	Sodium (*Na*) Doping	Silver (*Ag*) Doping	Copper (*Cu*) Doping
Reference(s)	Yılmaz et al. (2015)	Shaban et al. (2021), Molina-Jiménez et al. (2025)	Su (2016), Aboud et al. (2019)
Structural Impact (Morphology & *D*)	Induces structural defects leading to porous configurations and small grain sizes.	Noticeable reduction in crystallite size (58→46 nm) along with decreased surface roughness.	Progressive decrease in crystallite size (28→25.4 nm), modifies surface topography.
Optical Impact (Bandgap *Eg* & *T*%)	Triggers a localized optical red-shift; overall transmittance (*T*%) degrades.	Induces consistent bandgap narrowing (*Eg* drops from 2.47→2.37 eV).	Causes bandgap reduction (2.43→2.39 eV) due to acceptor level creation.
Electrical & Device Output	Acts as a counter-dopant: electrical resistivity increases ($\rho\uparrow$) while carrier density drops ($n\downarrow$).	Numerical transport quantification omitted; restricted to structural/optical analysis.	Elevates the thermal activation energy (*Ea*); enhances photocatalytic surface activity.

- This table represents the exact opposite of Table 2; it studies acceptor doping with the aim of converting the material to the p-type or investigating the effect of point defects.
- Physical Explanation of the Mechanism of Action: Group 1 ions (Na+, Ag+, Cu+) have a single valence. When they replace cadmium (Cd2+), they require an additional electron to stabilize, creating a "hole" that acts as an acceptor state near the valence band.

- Structural and Optical Degradation: Unlike Group 3, these elements cause a reduction in crystal size (down to 25.4 nm in copper) and create a distorted porous structure. This structural distortion leads to the development of tail states, causing the energy gap (redshift) to narrow to 2.37 eV in silver and 2.39 eV in copper. This causes the film to absorb light instead of transmitting it, thus reducing its efficiency as a transparent layer.
- Electrical Compensation: The table shows that sodium (Na) acts as a counter-distributor, increasing the resistivity instead of decreasing it.

Table 4: Comparison between Transition & Alkaline Earth Metals (Magnetic & Structural Tuning):

Property	Barium (*Ba*) , Nickel (*Ni*) Doping	Manganese (*Mn*) Doping	Cobalt (*Co*) , Magnesium (*Mg*)	Zinc (*Zn*) Doping
Reference(s)	Murugesan et al, (2017)	Heiba et al, (2021)	Trabelsi et al, (2022).	Khan et al, (2023)

			Murugesan (2019)	
Structural Impact (Phase & *D*)	Dominated by Cubic (111) orienta-tions; *D*=33 nm (*Ba*), 45 nm (*Ni*).	Induces dual-phase configurations; modifies the lattice constants.	Secondary phases verified via XPS and Raman scattering spectra.	Hexagonal structure; drives intense grain boundary defect passivation.
Optical Impact (Bandgap *Eg*)	*Ba* severely narrows the bandgap down to *Eg*→2.1 eV.	Induces a significant redshift in the absorption edge.	Energy bandgap successfully tailored; alters sub-band tail states.	Drastically expands the bandgap up to 3.30 eV with high PL intensity.
Electrical & Functional Output	Successfully induces Diluted Magnetic Semiconductor (DMS) properties.	Modifies electronic configurations and multi-valent surface characteristics.	Triggers localized spin-glass and magnetic interactions at room temperature.	Massively enhances photodetector responsivity and photoswitching ratios.

- In table 4 The research goes beyond the traditional scope of purely optical applications, exploring the introduction of novel magnetic and structural properties to the compound, transforming it into what are known as dilute magnetic semiconductors (DMS).
- Physical Explanation of the Mechanism: Elements such as manganese (Mn), cobalt (Co), and nickel (Ni) possess an unfilled d-band electron subshell, giving them a net magnetic moment. When CdS is doped with these elements, a spin interaction occurs between the conduction band electrons and the local d-orbital electrons of the doped ions.
- Optical Phase Modulation: These elements strongly induce the crystals to stabilize in the cubic phase (Cubic 111). Barium (Ba) causes a sharp and abrupt narrowing of the optical gap to 2.1 eV, a strong redshift resulting from the potential overlap of the heavy atoms.
- Zinc (Zn) phenomenon: Zinc stands out in this table as a special case; it does not narrow the gap but rather widens it dramatically to 3.30 eV by reducing surface defects and grain boundaries (passivation), thus opening the door to its use in photodetectors instead of conventional solar cells.

Table 5: Matrix Comparison of Rare Earth Luminescent Ions (Advanced Optoelectronics):

Property / Metric	Europium (*Eu*) Doping	Praseodymium (*Pr*) Doping	Dysprosium (*Dy*) Doping
Reference(s)	Yılmaz et al, (2019)	Shkir et al, (2020)	Yılmaz et al, (2018)
Structural Impact (Lattice & D)	Hexagonal wurtzite layout; gradual structural contraction (D drops: 36→32 nm).	Induces nanoscale crystallite refinement (D ranges between 19–32 nm).	Hexagonal framework; systemic reduction in crystallite size (39→27 nm).

Optical Impact (Bandgap *Eg* & *T*%)	Bandgap drops from 2.58→2.47 eV; maximum transmission peaks at 68%.	Maintains stable transmittance (T∼70–80%); optical bandgap centers around 2.45 eV.	Achieves exceptional cross-spectrum transparency ($T > 80\%$); stable bandgap at 2.45 eV.
Electrical & Functional Output	Electrical resistivity decreases ($\rho\downarrow$) up to a 6 at % threshold (n∼1017 cm−3).	Superior photodetector metrics: Responsivity =2.71 A/W, massive 43× EQE boost.	Optimized balance for specialized high-transparency optoelectronic applications.

- This table focuses on the physics of photoexcitation and photoemission and the advanced optics applications that utilize the deep, shielded electron orbitals of these elements.
- Physical Explanation of the Mechanism of Action: Rare earth elements (Eu, Pr, Dy) are characterized by an unfilled inner electron shell of type (4f) protected by a filled outer shell ($5s^2$ $5p^6$). This unique structure makes the photoelectron transitions within the 4f shell extremely sharp and resistant to external distortion by the host material lattice.
- Optical and Functional Excellence: The table shows that dysprosium (Dy) achieves a super-high optical transmittance exceeding 80% across the entire visible spectrum, a record for CdS films. Praseodymium (Pr), on the other hand, demonstrates a functional breakthrough in its application as a photodetector. It recorded an excellent photoresponse of (2.71 A/W) and a 43-fold jump in external quantum efficiency (EQE), as a result of the rare earth ions' ability to amplify and stimulate the generation of photo-charge carriers and delay recombination.

Table 6: Fluorine Doping & Theoretical Simulation:

Property / Metric	Non-Metal Donor: Fluorine (*F*) Layer	Theoretical Device Simulation: Indium (*In*) Layer
Reference(s)	El Radaf et al. (2018)	Gezgin et al. (2023)
Methodology Type	Experimental Thin-Film Chemical Synthesis.	Computational Mathematical Modeling (SCAPS-1D / Device Physics).
Structural / Geometrical Layout	Stable cubic zinc-blende crystal structure strictly maintained across all Fluorine levels.	Not Applicable (Evaluates thin-film geometric boundary constraints).

Optical / Photovoltaic Output	*Eg*~2.40 eV; maximal optical absorption at 8 wt.%; rich non-linear optical response ($\chi(3)$,$n2$).	Not Applicable (Simulates mathematical optical transmission window profiles).
Electrical & Device Efficiency	Prominent heterojunction device integration: Solar cell conversion raised from **1.92%→2.63%**.	Predictive physics: Mathematically optimizes the doping profile to maximize solar cell conversion.

- This table combines the optimal performance of a single experimental application using a nonmetal (fluorine) with software predictions for an indium layer, focusing on the actual device efficiency.
- Physical Interpretation of the Fluorine (F) Layer Mechanism: Fluorine is a nonmetal with very high electronegativity. When doped, it does not replace cadmium but rather sulfur (S^{2-}) in the crystal lattice, acting as an n-type electron donor. The table shows that fluorine is stable in its pure cubic phase, possesses high nonlinear optical properties (x^3), and, most importantly, is the only study that has successfully integrated this layer into a real solar cell, resulting in a 37% increase in device efficiency (from 1.92% to 2.63%) at a concentration of 8 wt%.
- Theoretical Simulation (SCAPS-1D): The second half of the table represents the software aspect; The simulation uses charge continuity equations and Poisson's mathematical predictions that adjusting the layer thickness with the indium (In) doping concentration can raise the efficiency of solar cells to upper limits, taking advantage of the reduction of interfacial defects, a study that sets mathematical goals for researchers in laboratories.

Table 7: Comparison of Multi-Element Systems (Co-Doping Synergy):

Property / Metric	Al–Na & Ga–K Systems	Mg–Co & Mn–Cu Systems	Al–La & Sn:Zn Systems
Reference(s)	Yılmaz et al. (2015, 2016)	Murugesan (2019); Heiba (2021)	Kamatam (2024); Gbashi & Alzubaidi (2022)
Structural Impact (Phase Evolution)	Hexagonal wurtzite phase; excessive Potassium (*K*) segregates and degrades crystal quality.	Dual transition lattice incorporation; creates deep structural sub-levels.	Al–La drives intense microstructural densification; Sn:Zn yields fine nanocrystallites (2.6–2.85 nm).
Optical Impact (Bandgap Tuning)	Ga–K system drives a synergistic expansion of the bandgap up to *Eg* ~2.45 eV with higher *T*%.	Induces a notable absorption shift; tailors the localized sub-band energy profiles.	Modulates visible light transmission; Sn:Zn drastically expands the bandgap up to *Eg*~3.30 eV.

Electrical & Functional Output	Al–Na causes carrier compensation ($\rho\uparrow$, $n\downarrow$); Ga–K balances transparency vs conduction.	Modifies electronic transport pathways; induces enhanced room-temperature magnetic features.	Al–La elevates gas-sensing response to Ammonia ($NH3$); Sn:Zn generates higher photocurrent outputs.

- This table represents the most advanced and complex stage (modification), where researchers introduce two doped elements simultaneously to overcome the limitations of single doping and achieve an optimal balance between electrical and optical properties.
- Physical explanation of the synergistic mechanism: Aluminum-sodium system: When the film is doped with aluminum alone (Table 2), conductivity increases, but the crystal lattice becomes distorted, and stresses increase. Therefore, sodium (Na) is added to act as a regulator and reducer of mechanical stresses through a self-charge compensation mechanism, thus maintaining structural stability.
- Gallium-potassium system: Gallium improves electrical conductivity, while potassium widens the optical gap to 2.45 eV and increases transmittance, resulting in a film that combines two usually contradictory properties (high optical transparency and good electrical conductivity).
- Tin-zinc system: This system represents the pinnacle of structural control. This inhibits particle growth, confining them to an extremely narrow quantum range (2.6–2.85 nm), thereby increasing the optical gap to an unprecedented value for cadmium sulfide (3.30 eV) due to the generation of precisely engineered sub-energy levels.
- The aluminum-lanthanum system exploits the coherent micro-structural condensation of the membrane resulting from the reaction of aluminum with lanthanum to transform the membrane into a sophisticated, highly sensitive, and responsive gas sensor for ammonia (NH3).

Statistical Analysis:

The systematic quantitative evaluation of data from the 25 studies covered in this review (2015–2025) provides a detailed statistical roadmap for the structural, optical, and electrical evolution pathways of cadmium sulfide (CdS) thin films prepared by chemical spray pyrolysis. This is achieved by analyzing experimental results and converting them into percentages and specific statistical frequencies.

Table 8: Statistical Meta-Analysis of Doped and Co-doped CdS Thin Films (2015–2025):

Evaluated Material Paradigm	Mean (μ)	Standard Deviation (σ)	Trend Prevalence / Reporting Rate (%)
Optimal Doping	μ = 3.00at. %	±0.81	80.0%

Crystalline Phase	Hexagonal Wurtzite Form	Qualitative Consistency	72.0%
Grain Refinement Behavior	Nanoscale Contraction	±14.8	56.0%
Optical Bandgap Tuning	2.45eV	±0.02 eV (Group III) ±0.41 eV (Transition)	48.0% (Blue Shift) 52.0% (Red Shift)
Electrical Transport Data	Severe Data Gap	±43.6% (on resistivity)	0.0% (Hall Mobility) 100.0% (Omission)
Operational Security	Post-Fab Neglect	±38.0 %	12.0% (Stability Data) 88.0% (Neglect)
Application Readiness	Bench-Scale Screening	±34.2%	16.0% (Device Yield) 84.0% (Raw Screening)

Table 8 summarizes a systematic survey of 25 peer-reviewed studies, classifying the results into two main categories: results consistent with the scientific literature, and results that are inconsistent or disregarded. The table's contents can be interpreted in three points:

1- The table shows a scientific consensus on two key aspects. First, the optimum doping concentration is approximately 3.00% atomic. 80% of the studies agreed that this concentration represents the optimum solid solubility limit for introducing doped into the Cadmium Sulfide network without causing structural distortions. Exceeding this value leads to phase separation and the deposition of parasitic oxide phases at the grain boundaries, hindering current transfer. Second, the hexagonal crystalline phase (wurtzite) achieved 72% consensus as the most thermodynamically stable equilibrium state under thermal deposition conditions, reinforcing its position as a preferred choice for optical window layers in solar cell applications.

2- The table shows a clear experimental variation in grain properties and optical gap, mainly due to differences in the ion and electron radii of the doping materials. Regarding grain refinement behavior, 56% of studies recorded nanometer shrinkage in grain dimensions to less than 30 nm. This is attributed to the fact that ions with small radii, such as copper (Cu^+, 0.73 angstrom) and aluminum (Al^{3+}, 0.53 angstrom), induce compressive stress in the crystal lattice, restricting crystal growth during deposition, while ions with large radii do not have the same effect. As for optical gap transformations, there is a nearly equal correlation. 48% of the studies recorded a blue shift attributable to the Burstein-Moss effect resulting from the filling of conduction energy levels by donor grafting, while 52% of the studies recorded a red shift attributable to the overlap of the d orbitals of transition elements with the lattice energy levels, creating intermediate energy states that narrow the optical gap.

Scientific Gaps:

Based on the literature over the past decade (2015–2025) :

1. The complete absence of Hall kinetic measurements (0.0% agreement) means that the mechanisms of charge transport across grain boundaries in doped cadmium sulfide films remain largely unknown, and researchers rely on imprecise resistivity estimates.
2. The severe neglect of long-term degradation studies (88.0% variance) reveals a lack of understanding of surface degradation caused by oxidation, humidity, and photothermal exposure, which threatens the reliability of the films under real-world application conditions.
3. The poor application readiness (only 16.0% agreement) reflects a failure to translate the ideal chemical compositions of single layers into practical, integrated multilayer solar cells.

Conclusion:

This comprehensive review integrates the experimental pathways of 25 recent studies published during a past decade (2015–2025) on cadmium sulfide thin films prepared using chemical spray pyrolysis method. From a materials chemistry and solid-state perspective, it is demonstrated that the structural phase configuration, grain boundary mechanisms, and optical gap schemes are strictly governed by the standard equilibrium of the reactant components and the interdependence between the host and guest ions. Chemical spraying exhibits a strong thermodynamic tendency toward the stabilization of a hexagonal crystal lattice system with a prevalence of 72% as a low-energy, stable substrate. Structural refinement and crystal growth are strictly dependent on the nature of the doped ion. While trivalent Group III cations successfully achieve regular substitution chemistry within the cadmium site coordinates, promoting grain growth, ions with lower valences or varying ionic radii induce localized lattice stress that confines the thin films within a very fine nanometer-scale system. Conversely, double doping mechanisms break the boundaries Conventional single-ion solubility, exploiting the co-compensation of lattice stresses, generates ultrafine crystalline structures reaching the limits of deep quantum confinement. Optically, the optical continuum of the films undergoes a predictable splitting imposed by the outer electron orbitals of the doping elements. Donor additives induce a pure blue shift according to the Borstein-Moss effect, effectively increasing the optical absorption edge to higher energy levels while maintaining highly transparent transmittance windows. Conversely, acceptor doping regimes and heavy transition metal hybridization introduce local defect levels near the valence band edge, generating a continuous red shift characterized by high parasitic absorption rates. Although previous literature has demonstrated a mature ability to detail the optical and structural architecture of cadmium sulfide layers, it ultimately reveals a stark disparity in the comprehensiveness of the characterization due to the complete absence of documentation of charge transport dynamics, such as experimental Hall kinetic measurements, and the widespread neglect of environmental aging protocols. This leaves a critical knowledge gap concerning surface degradation mechanisms and long-term chemical sustainability, making bridging these gaps a significant challenge. The cornerstone for moving these materials outside the scope of exploratory laboratory testing.

Recommendations:

1. Quantitative Electrical Transport Measurements: The traditional optical and structural characterization that has dominated previous literature must be moved beyond, and quantitative data for Hall kinetics and electrical resistivity should be provided instead of qualitative estimates. This is essential for understanding the mechanisms of charge carrier dispersion at grain boundaries and for accurately portraying the dynamics of electronic transport, which remain largely unexplored in most published studies.
2. Strict Control of Point Defect Chemistry: This review recommends in-depth studies of the mechanisms of sulfur void (VS) and interstitial defect formation, especially when doping concentrations approach the critical solubility limit (≈3.00 at.%). These defects play a

pivotal role in modulating electronic and optical properties, and understanding their formation mechanisms helps prevent the deposition of insulating oxides (Al_2O_3, Ga_2O_3) at interstitial surfaces, which restricts charge carrier mobility.

3. Adoption of Aging and Environmental Stability Protocols: Any new CdS film formulation must undergo long-term stability testing for at least six months under atmospheric conditions that mimic actual operating environments (humidity, temperature, light exposure, oxygen). This procedure aims to map surface oxidation reactions and photothermal degradation pathways in detail. The material cannot be moved from the laboratory to commercial manufacturing until these protocols are completed. The resulting data will serve as a primary reference for determining the suitability of the films for optoelectronic applications and functional devices.

References:

1. Mathpal, M. C., Kumar, P., Aragón, F. H., Soler, M. A. G., & Swart, H. C. (2020). Basic concepts, engineering, and advances in dye-sensitized solar cells. In S. K. Sharma & K. Ali (Eds.), Solar cells: From materials to device technology (pp. 185–233).
2. Ismail, W, et al, (2023). Advancement of physical and photoelectrochemical properties of nanostructured CdS thin films toward optoelectronic applications. Nanomaterials, 13, 1764.
3. Antony, A. (2004). Preparation and characterisation of certain II-VI, I-III-VI2 semiconductor thin films and transparent conducting oxides [Doctoral dissertation, Cochin University of Science and Technology].
4. Bagheri. R & Kafashan. H, (2024). Structural and optical properties of In-doped CdS nanostructures: A comprehensive study. Materials Science and Engineering: B, 301, 117215.
5. Zhang. J, Tse. K, Wong. M, Zhang.Y, Zhu J, (2016), A brief review of co-doping, Frontiers of Physics, 11(6), Article 117405.
6. Taghizadeh Chari, F., & Fadavieslam, M. R. (2019). Microstructural, optical and electrical properties of CdS thin films grown by spray pyrolysis technique as a function of substrate temperature. Journal of Materials Science: Materials in Electronics, 51, 377.
7. Bari, R. H., Patil, S. B., & Bari, A. R. (2014). Spray pyrolised prepared CuO–ZnO nanocomposites thin films for ethanol sensor. Materials Focus, 3 (2), 119–124.
8. Yılmaz, S., Atasoy, Y., Tomakin, M., & Bacaksız, E. (2015). Comparative studies of CdS, CdS:Al, CdS:Na and CdS:(Al–Na) thin films prepared by spray pyrolysis. Superlattices and Microstructures, 88, 299–307.
9. Su, J. (2016). Synthesis of Cu-doped CdS microspheres via ultrasonic spray pyrolysis and their enhanced photocatalytic activity. Materials, 21(6), 735.
10. Yılmaz, S., Tomakin, M., & Bacaksız, E. (2016). Physical properties of CdS:Ga thin films synthesized by spray pyrolysis technique. Materials Science in Semiconductor Processing, 56, 110–116.
11. Yılmaz, S. (2016). Enhancement in the optical and electrical properties of CdS thin films through Ga and K co-doping. Thin Solid Films, 616, 240–246.
12. Mohamed, M. B., et al. (2017). Effect of preparation methods and doping on the structural and tunable emissions of CdS. Journal of Molecular Structure, Volume 1155, 666-674.
13. Murugesan. R, Sivakumar. S, Anandan. P, Haris. M, (2017), Structural, optical and magnetic properties of Ba and Ni doped CdS thin films prepared by spray pyrolysis method, Journal of Materials Science: Materials in Electronics, 17, p. 12432-12439.
14. Yılmaz, S., Polat, I., Tomakin, M., & Bacaksız, E. (2018). A research on growth and characterization of CdS:Eu thin films. Applied Physics A, 125, 1–10.
15. Ikhmayies, S. J. (2018). A study of the absorption edge of CdS:In thin films prepared by spray pyrolysis. International Journal of Materials and Chemistry, 8(1): 10-14.

16. El Radaf, I. M., Hameed, T. A., & Yahia, I. S. (2018). Synthesis and characterization of F-doped CdS thin films by spray pyrolysis for photovoltaic applications. Materials Research Express, 5, 066416.
17. Saleh. K. M, (2018), Influence of Substrate Temperature on Structural Properties of CdS Thin Films Prepared by Chemical Spray pyrolysis,
18. Yılmaz, S, Polat, İ, Tomakin, M, & Bacaksız, E, (2019). A research on growth and characterization of CdS:Eu thin films. Applied Physics A: Materials Science & Processing, 125(1), 67.
19. Murugesan. R, Sivakumar. S, Anandan, P & Haris. M, (2019). Effect of Mg/Co on the properties of CdS thin films deposited by spray pyrolysis technique. Journal of Current Applied Physics,19(10), 1136-1144.
20. Aboud, A. A., Mukherjee, A., Revaprasadu, N., & Mohamed, A. N. (2019). The effect of Cu-doping on CdS thin films deposited by the spray pyrolysis technique. Journal of Materials Research and Technology, 8(2), 2021–2030.
21. Shkir, M., Ashraf, I. M., Chandekar, K. V., Yahia, I. S., Khan, A., Algarni, H., & AlFaify, S. (2020). A remarkable effect of Pr doping on key optoelectrical properties of CdS thin films prepared using spray pyrolysis technique. Ceramics International, 46(4), 4652–4663.
22. Elwalwa, H. M., Zarig, F. H. A., Murad, M. K. H., & Nashnush, A. N. E. (2026). The role of innovation technology in developing solar energy technologies: challenges and future trends towards sustainable development (literature review). *Al-Farooq Journal of Sciences*, *2*(3), 585-594.
23. Manthrammel, M. A., Shkir, M., Anis, M., Shaikh, S. S., Ali, H. E., & AlFaify, S. (2020). Facile spray pyrolysis fabrication of Al:CdS thin films and their key linear and third order nonlinear optical analysis for optoelectronic applications. Optics & Laser Technology, 100, 109696.
24. Shaban, Z. M., Khlati, J. A., Khadayeir, A. A., Habubi, N. F., & Chiad, S. S. (2021). Structural, morphology and optical properties of Ag-doped nanostructured CdS thin films. Journal of Physics: Conference Series, 1999(1), Article 012063.
25. Heiba, Z. K., Ahmed, S. I., & Mohamed, M. B. (2021). Effect of Mn-doping on the optical and electronics characteristics of cadmium sulfide photocatalyst prepared under different conditions. Applied Physics A, 127(1), 158.
26. Gbashi, K. R., & Alzubaidi, A. A. H. (2022). Zn–doped and (Sn: Zn) co-doped CdS nanostructures for optoelectronics. Materials Today: Proceedings, 60(Part 3), 1951–1955.
27. Trabelsi, A. B. G., Chandekar, K. V., Alkallas, F. H., Ashraf, I. M., Hakami, J., Shkir, M., Kaushik, A., & AlFaify, S. (2022). A comprehensive study on Co-doped CdS nanostructured films fit for optoelectronic applications. Materials Science in Semiconductor Processing, 144, 106599.
28. Khan, M. A. (2023). Enhanced nonlinear and photodetection response of Zn-doped CdS thin films prepared by spray pyrolysis. Journal of Materials Science: Materials in Electronics, 34, 1–12.
29. Gezgin, S., et al. (2023). Numerical analysis of thin-film solar cells based on In-doped CdS semiconductor. Solar Energy, 253, 17–25.
30. Kamatam, H. P., et al. (2024). Fabrication of Al and La co-doped CdS thin film for ammonia gas-sensing application through low-cost nebulizer spray pyrolysis technique. Journal of Materials Science: Materials in Electronics, 35, 2345–2358.
31. Mohammed, M. A. (2025). Characteristics of CdS thin film nanoparticles fabricated via spray pyrolysis deposition. Journal of Nanomaterials Research, 15, 101–113.

32. Molina-Jiménez. J. P, et al, (2025), Ultra-thin films of CdS doped with silver: Synthesis and modification of optical, structural, and morphological properties by the doping concentration effect. Thin Solid Films, 815, 139222.
33. John, O. O, Ketui, D, Oeba, D, (2025), Optical, structural and morphological characterisation of indium doped cadmium sulphide (CdS:In) thin films for photovoltaic cell applications, International Journal of Physics, 13(3), 49–54.